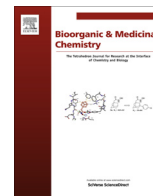




Since January 2020 Elsevier has created a COVID-19 resource centre with free information in English and Mandarin on the novel coronavirus COVID-19. The COVID-19 resource centre is hosted on Elsevier Connect, the company's public news and information website.

Elsevier hereby grants permission to make all its COVID-19-related research that is available on the COVID-19 resource centre - including this research content - immediately available in PubMed Central and other publicly funded repositories, such as the WHO COVID database with rights for unrestricted research re-use and analyses in any form or by any means with acknowledgement of the original source. These permissions are granted for free by Elsevier for as long as the COVID-19 resource centre remains active.



Dieckol, a SARS-CoV 3CL^{pro} inhibitor, isolated from the edible brown algae *Ecklonia cava*



Ji-Young Park^{a,b}, Jang Hoon Kim^a, Jung Min Kwon^a, Hyung-Jun Kwon^a, Hyung Jae Jeong^a, Young Min Kim^a, Doman Kim^b, Woo Song Lee^{a,*}, Young Bae Ryu^{a,*}

^a Infection Control Research Center, Korea Research Institute of Bioscience and Biotechnology, Jeongseup 580-185, Republic of Korea

^b School of Biological Science and Biotechnology, Chonnam National University, Gwangju 500-757, Republic of Korea

ARTICLE INFO

Article history:

Received 28 February 2013

Revised 11 April 2013

Accepted 12 April 2013

Available online 22 April 2013

Keywords:

Phlorotannin

SARS-CoV

Dieckol

Eckol

Ecklonia cava

ABSTRACT

SARS-CoV 3CL^{pro} plays an important role in viral replication. In this study, we performed a biological evaluation on nine phlorotannins isolated from the edible brown algae *Ecklonia cava*. The nine isolated phlorotannins (**1–9**), except phloroglucinol (**1**), possessed SARS-CoV 3CL^{pro} inhibitory activities in a dose-dependently and competitive manner. Of these phlorotannins (**1–9**), two eckol groups with a diphenyl ether linked dieckol (**8**) showed the most potent SARS-CoV 3CL^{pro} *trans/cis*-cleavage inhibitory effects (IC₅₀s = 2.7 and 68.1 μM, respectively). This is the first report of a (**8**) phlorotannin chemotype significantly blocking the cleavage of SARS-CoV 3CL^{pro} in a cell-based assay with no toxicity. Furthermore, dieckol (**8**) exhibited a high association rate in the SPR sensorgram and formed extremely strong hydrogen bonds to the catalytic dyad (Cys145 and His41) of the SARS-CoV 3CL^{pro}.

© 2013 Elsevier Ltd. All rights reserved.

1. Introduction

Brown algae have long been used traditionally as foodstuffs and folk medicines in Asian countries. Recently, a commercially available *Ecklonia cava* extract was approved as a new dietary ingredient (NDI) by the U.S. Food and Drug Administration (FDA) in 2008 (FDA-1995-S-0039-0176). Marine algae have been identified as rich sources of structurally diverse bioactive compounds with great pharmaceutical and biomedical potential. *Ecklonia cava* (Laminariaceae) is an edible brown alga that grows abundantly in the subtidal regions of Jeju Island, Korea. *E. cava* is used to produce food ingredients, animal feed, fertilizers, and folk gynecopathic medicines.¹ *E. cava* contains a variety of compounds, including carotenoids, fucoidan, and phlorotannins, that show different biological activities.^{2,3} The phlorotannin components, which are oligomeric polyphenols with phloroglucinol units, are responsible for the pharmacological activities of *E. cava*.⁴ *Ecklonia* species have been used extensively as traditional medicines for the treatment of goiter, scrofula, urinary diseases, stomach ailments, hemorrhoids, boils, constipation, and postpartum women.⁵ Previous studies have

Abbreviations: SARS, severe acute respiratory syndrome; CoV, coronavirus; IC₅₀, the inhibitor concentration leading to 50% activity loss; K_i, inhibition constant; K_d, dissociation constant; NMR, nuclear magnetic resonance; SPR, surface plasmon resonance; Luc, luciferase.

* Corresponding authors. Tel.: +82 63 570 5005 (W.S.L.); tel.: +82 63 570 5171; fax: +82 63 570 5239 (Y.B.R.).

E-mail addresses: wslee@kribb.re.kr (W.S. Lee), ybryu@kribb.re.kr (Y.B. Ryu).

presented a wealth of evidence showing that *E. cava* exhibits antioxidant,⁶ anticancer,⁷ immunomodulatory,^{8,9} and tyrosinase inhibitory activity.¹⁰ *E. cava* also exhibits anti-virus activities against HIV-1 reverse transcriptase¹¹ and influenza virus neuraminidase.¹² However, to the best of our knowledge, there have been no reports of the phlorotannins from *E. cava* eliciting severe acute respiratory syndrome coronavirus (SARS-CoV) 3C-like proteinase (3CL^{pro}) inhibitory activity.

SARS is a life-threatening form of atypical pneumonia caused by infection with a novel human coronavirus (SARS-CoV).^{13–15} Its 3CL^{pro}, a chymotrypsin-like cysteine proteinase essential for viral replication, has been recognized as a key target for anti-SARS drug design. The active site of SARS-CoV 3CL^{pro} contains a catalytic dyad composed of Cys145 and His41, where the cysteine residue (Cys145) acts as a nucleophile and the histidine residue (His41) acts as the general acid–base in the proteolytic process.¹⁶ Until now, SARS-CoV 3CL^{pro} inhibitors have been reported from both synthetic peptidyl compound libraries and natural product-derived libraries.¹⁷ The synthetic inhibitory compounds include C₂-symmetric diols,¹⁸ quinolinecarboxylic acids,¹⁹ and anilides.²⁰ The natural-derived inhibitors include betulinic acid,²¹ indigo,²² aloemodin,²² quinone-methide triterpenoids²³ and biflavonoids amentoflavones.²⁴

The aim of this present study was to investigate a SARS-CoV 3CL^{pro} inhibitor isolated from *E. cava*. We characterized the anti-SARS-CoV 3CL^{pro} effect of isolated phlorotannins from *E. cava* using cell-free cleavage and cell-based cleavage assays. To examine the

trans-cleavage of SARS-CoV 3CL^{pro} in the cell-free assay, the proteolytic activity of 3CL^{pro} was tested against a fluorogenic substrate (Dabcyl-KTSAVLQSGFRKME-Edans) and analyzed with a fluorescence resonance energy transfer (FRET) assay. The *cis*-cleavage of SARS-CoV 3CL^{pro} was determined with a cell-based assay; the in-frame construction of 3CL^{pro}, the substrate (SAVLQSGFRK), and luciferase (Luc) was transfected into the Vero cells, and the *cis*-cleavage activities of SARS-CoV 3CL^{pro} were determined using a luciferase assay. We also assessed the effect of the inhibitor on the SARS-CoV 3CL^{pro} interaction using a surface plasmon resonance (SPR) analysis and a binding model.

2. Results and discussion

2.1. Preparation of SARS-CoV 3CL^{pro} and effect of isolated phlorotannins on SARS-CoV 3CL^{pro} *trans*-cleavage assay

Because of the numerous functions and requisite roles of cysteine proteases in viral replication and pathogenesis, they may serve as attractive targets for antiviral drugs. The severe acute respiratory syndrome (SARS) coronavirus (CoV) depends on a chymotrypsin-like cysteine protease (3CL^{pro}) to process the translated polyproteins into functional viral proteins. This enzyme is a target for potential anti-SARS drugs. Ultimately, our goal is to develop a naturally derived SARS-CoV 3CL^{pro} inhibitor for use as anti-SARS drug. Our first step toward this goal was to express and purify SARS-CoV 3CL^{pro} from *E. coli* BL21 (DE3) CodonPlus-RIL cells as described in Section 2. The purified protease ran at approximately 33 kDa on sodium dodecyl sulfate–polyacrylamide gel electrophoresis (SDS–PAGE) with greater than 90% purity. The purified 3CL^{pro} from *Escherichia coli* cells had a specific activity of 32.0 ± 5.2 μM towards the Dabcyl-KTSAVLQSGFRKME-Edans substrate.

A bioassay-guided investigation of the ethanol extract of *Ecklonia cava* resulted in the isolation of nine phlorotannins: phloroglucinol (**1**), triphloretol A (**2**), eckol (**3**), dioxinodehydroeckol (**4**),

Table 1

Inhibitory effects of isolated phlorotannins (**1–9**) on the cell-free cleavage activity of SARS-CoV 3CL^{pro}

Compounds	Cell-free <i>trans</i> -cleavage	
	IC ₅₀ ^a (μM)	Inhibition type (K _i , μM)
1	>200	NT ^b
2	164.7 ± 10.8	NT
3	8.8 ± 3.5	Competitive (8.2 ± 0.9)
4	158.3 ± 8.2	NT
5	13.3 ± 0.8	Competitive (24.0 ± 1.5)
6	42.1 ± 2.2	Competitive (19.3 ± 1.4)
7	22.5 ± 4.6	Competitive (63.5 ± 7.1)
8	2.7 ± 0.6	Competitive (2.4 ± 0.2)
9	16.7 ± 3.3	Competitive (10.6 ± 1.0)

^a All compounds were examined in a set of triplicates experiment; IC₅₀ (50% inhibitory concentration) values of compounds represent the concentration that caused 50% enzyme activity loss.

^b Not tested.

2-phloroeckol (**5**), 7-phloroeckol (**6**), fucodiphloroethol G (**7**), dieckol (**8**), and phlorofucofuroeckol A (**9**) (Fig. 1). First, we examined the effect of nine phlorotannins **1–9** on the cell-free SARS-CoV 3CL^{pro} *trans*-cleavage assay. The percent inhibition at 200 μM concentrations of compounds **1–9** was initially determined, and the results are reported in Table 1. As shown in Table 1 and Figure 2A, all of the phlorotannins investigated, except phloroglucinol (**1**), exhibited a dose-dependent inhibitory effect on 3CL^{pro} hydrolysis with IC₅₀ values ranging from 2.7 to 164.7 μM against cell-free 3CL^{pro} *trans*-cleavage. As the concentrations of the inhibitors were increased, the residual SARS-CoV 3CL^{pro} activity decreased dramatically. All inhibitors exhibited a similar relationship between enzyme activity and enzyme concentration. As an example, the relevant data for dieckol (**8**) is illustrated in Figure 2B. Plots of the residual enzyme activity versus enzyme concentration at various concentrations of dieckol (**8**) yielded a series of straight lines with

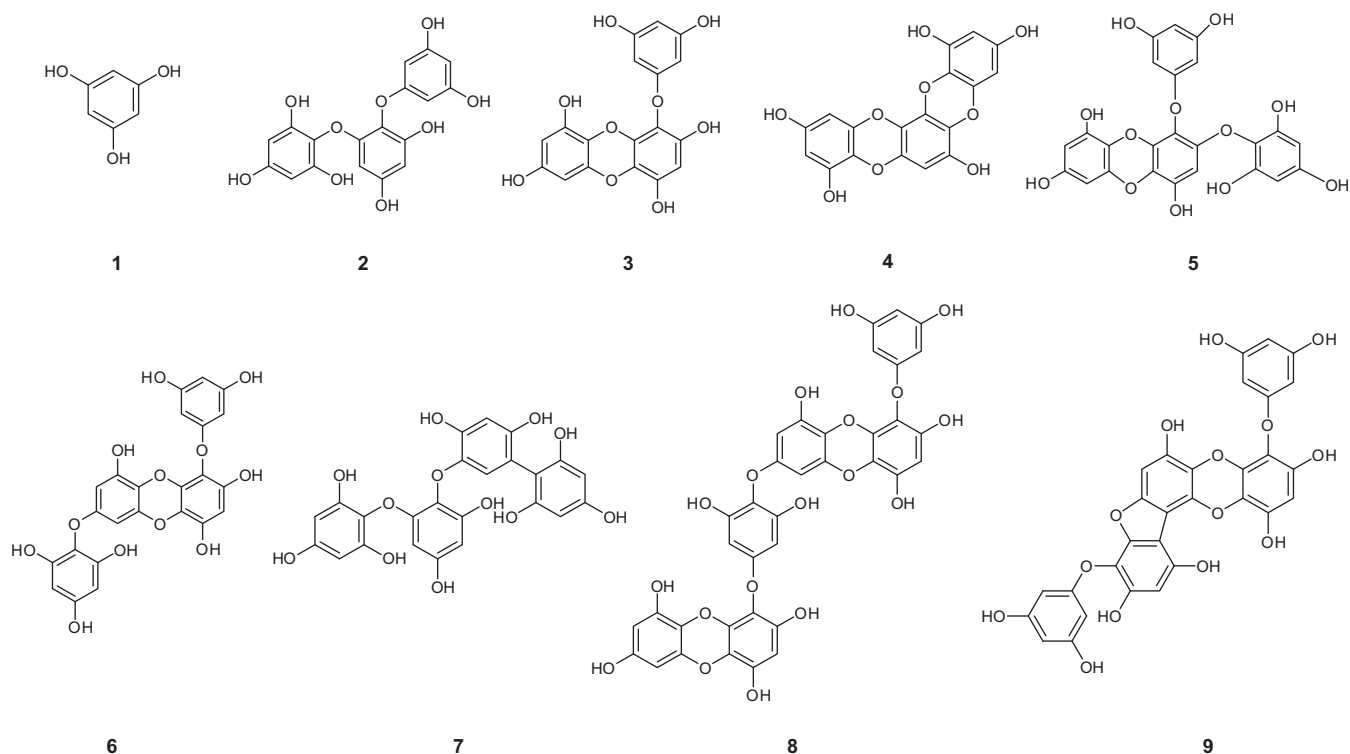


Figure 1. Chemical structures of isolated phlorotannins from *Ecklonia cava*.

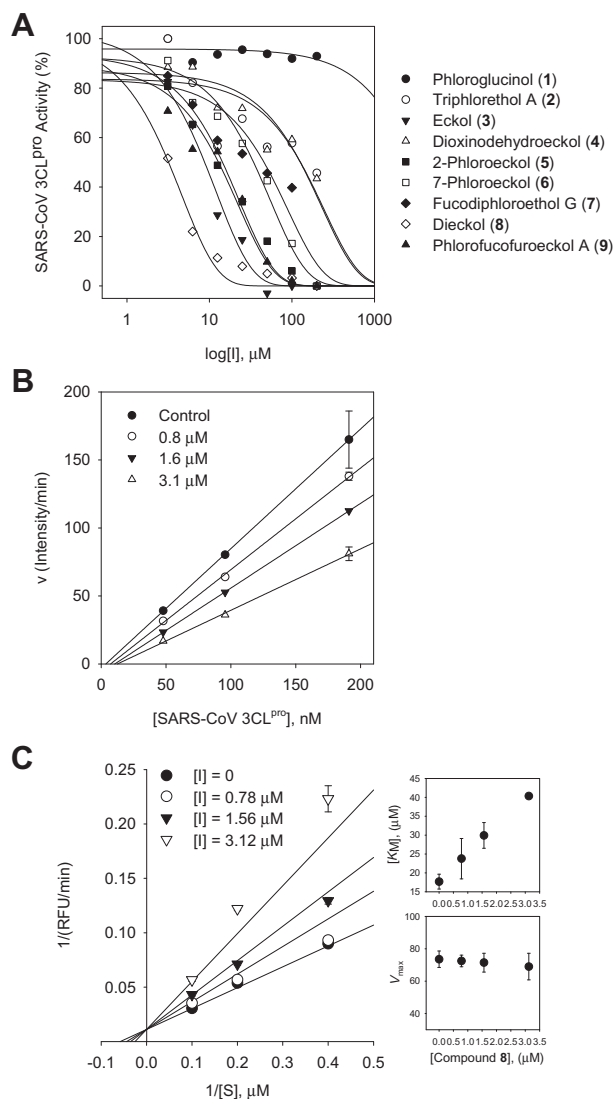


Figure 2. (A) Effects of compounds 1–9 on the activity of SARS-CoV 3CL^{pro} for proteolysis of substrate. (B) The catalytic activity of SARS-CoV 3CL^{pro} as function of enzyme concentration at different concentrations of compound 8. (C) Lineweaver–Burk plots for inhibition of dieckol (8) on SARS-CoV 3CL^{pro} for the proteolysis of substrate. The values of K_M and V_{max} on the concentrations of compound 8 (inset).

an axis intercept of 0, indicating that all inhibitors are reversible. Augmenting the concentration of dieckol (8) reduced the slopes of the lines. Of the isolated phlorotannins, eckol (3, $IC_{50} = 8.8 \mu\text{M}$) and dieckol (8, $IC_{50} = 2.7 \mu\text{M}$) displayed remarkable inhibitory activity against SARS-CoV 3CL^{pro} cell-free cleavage.

2.2. Biological evaluation, structure–activity relationship, and discussion of isolated phlorotannins

The inhibition activity was slightly affected by subtle changes in structure. Initially, we compared a closed-chain trimer of phloroglucinol (3, eckol) with an opened-chain trimer of phloroglucinol (2, triphloretol A), and we found that the activity of eckol ($IC_{50} = 8.8 \mu\text{M}$) was 20-fold higher than that of the trimer itself ($IC_{50} = 164.7 \mu\text{M}$). Replacement of the 3,5-dihydrophenoxy group by a dioxinodehydro group (4, $IC_{50} = 158.3 \mu\text{M}$) led to weaker inhibition compared to 3; however it was still more active than 2. Similar to this relationship, substitution of the 3,5-dihydrophenyl

group on the opened-chain trimer that formed a biaryl linkage tended to increase the activity (7, $IC_{50} = 22.5 \mu\text{M}$ vs 2, $IC_{50} = 164.7 \mu\text{M}$). However, substitution of the 3,5-dihydrophenoxy group of eckol yielded the tetrameric phlorotannins 4–6 with reduced activities. When we compared a series of phloroeckols (5 and 6), we found that introduction a 3,5-dihydrophenoxy substituent at the 2C-position of the 3,5-dihydrophenoxy group (phloro-) increased the inhibitory activity ~3-fold; 2-phloroeckol (5) had an $IC_{50} = 13.3 \mu\text{M}$ and 7-phloroeckol (6) had an $IC_{50} = 42.1 \mu\text{M}$. Interestingly, blocking of one of the hydroxy units (C7) on the A ring, which contains a five-membered closed ring, appear to exert a variable (9, $IC_{50} = 16.7 \mu\text{M}$) but not insignificant effect on the activity. As evidenced from the SARS-CoV 3CL^{pro} inhibition data, the eckol structure is essential and crucial for good inhibition of 3CL^{pro}. Most importantly, we found that dieckol (8), which possesses two eckol groups linked through a diphenyl ether, showed the most potent SARS-CoV 3CL^{pro} inhibitory activity ($IC_{50} = 2.7 \mu\text{M}$). In addition, the inhibitory effect of dieckol (8) was comparable to that of a naturally derived quinone-methide triterpene ($IC_{50} = 2.6 \mu\text{M}$), which we isolated during our previous investigation on 3CL^{pro} inhibitors from *Tripterygium regelii*.²⁴ Dieckol (8) showed 30-, 50-, and 60-fold greater activities than the positive control, hesperetin (60 μM), daidzein (105 μM), and aloemodin (132 μM), respectively, previously reported by Lin and co-workers.²² To the best of our knowledge, this is the first report on the biological activities of phlorotannins isolated from *E. cava* toward SARS-CoV 3CL^{pro}.

Next, we studied the kinetic mechanism of the interaction of these inhibitors with SARS-CoV 3CL^{pro}. The enzymatic activity was measured with a series of substrate concentrations and various inhibitor concentrations. The inhibition data were globally fit to all of the possible kinetic models. As shown in Figure 2C, the kinetic plots show that dieckol (8) has competitive inhibition profiles because the Lineweaver–Burk plot ($1/V$ vs $1/[S]$) is a series of straight lines with the same y-axis intercept for the SARS-CoV 3CL^{pro} inhibitors. All of the isolated inhibitors exhibited the same mode of action for inhibition. The K_i values in Table 1 were calculated from the Dixon plots, which are useful for determining the K_i value of the inhibitor (see Supplementary data Fig. 4S). The predominant inhibition mode shown by the naturally occurring viral enzyme inhibitors was noncompetitive. Interestingly, the inhibition of SARS-CoV 3CL^{pro} by the phlorotannins isolated from *E. cava* was rarely competitive, encouraged us to further investigate this phenomenon with a more detailed biological study.

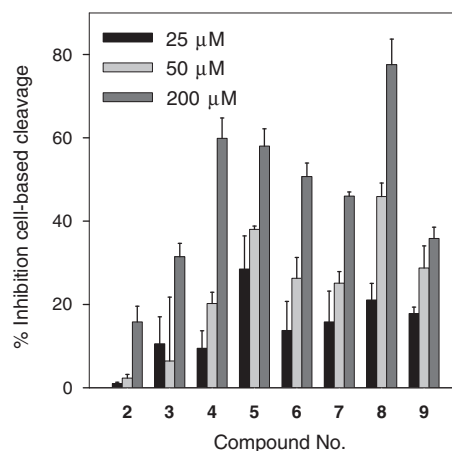


Figure 3. Inhibition of the cell-based *cis*-cleavage of the SARS-CoV 3CL^{pro} by the isolated phlorotannins (2–9).

Table 2Inhibitory effects of isolated phlorotannins (**1–9**) on the cell-based *cis*-cleavage activity of SARS-CoV 3CL^{pro}

Compounds	Cell-based cleavage		
	IC ₅₀ ^a (μM)	CC ₅₀ ^b (μM)	SI ^c
1	ND ^d	>200	ND
2	15% at 200 μM	>200	<1
3	30% at 200 μM	>200	<1
4	146.5 ± 12.5	>200	>1.4
5	112.2 ± 6.1	>200	>1.8
6	112.0 ± 5.8	>200	>1.8
7	177.1 ± 10.1	>200	>1.1
8	68.1 ± 2.2	>200	>2.9
9	174.6 ± 9.7	>200	>1.1

^a All compounds were examined in a set of triplicates experiment; IC₅₀ (50% inhibitory concentration) values of compounds represent the concentration that caused 50% enzyme activity loss.

^b All compounds were examined in a set of triplicates experiment; CC₅₀ (50% cytotoxic concentration) was the concentration giving half the OD_{570–630} nm of mock cells in MTT assay.

^c SI means selective index (CC₅₀/IC₅₀).

^d Not detected.

2.3. Effect of isolated phlorotannins on SARS-CoV 3CL^{pro} *cis*-cleavage assay

We subsequently performed the cell-based *cis*-cleavage assay to confirm the inhibitory activities of the isolated phlorotannins against SARS-CoV 3CL^{pro}. All of the tested phlorotannins, except **1–3**, exhibited dose-dependent cell-based SARS-CoV 3CL^{pro} *cis*-cleavage inhibitory activities. In the cell-based cleavage assay, the isolated phlorotannins **4–9** inhibited the *cis*-cleavage activity of the SARS-CoV 3CL^{pro} with IC₅₀ values ranging from 68 to 177 μM (Fig. 3 and Table 2) in a dose-dependent manner. Moreover, all of the phlorotannins were non-toxic to Vero cells with CC₅₀ values greater than 200 μM. Active phlorotannins were less effective when evaluated with the SARS-CoV 3CL^{pro} *cis*-cleavage assay than when evaluated by the cell-free *trans*-cleavage assay. The explanation for this result may be that several of the compounds cannot permeate the cellular membranes to reach the intracellular SARS-CoV 3CL^{pro}. The cell-based assay indicated that dieckol (**8**, IC₅₀ = 68.1 μM) is the most efficient at blocking the cleavage processing of the 3CL^{pro}, which agreed with the cell-free cleavage FRET assay data. Dieckol (**8**) showed a strong correlation between the effects on the cell-free and cell-based cleavage of the SARS-CoV 3CL^{pro}. In particular, dieckol (**8**) was more efficient at blocking the cleavage of 3CL^{pro} than indigo, sinigrin, beta-sitosterol, and aloemodin, which were previously reported plant-derived phenolic compounds.²² Although dieckol (**8**) is considerably less effective than hesperetin (IC₅₀ = 8.3 μM),²² it is the first report of a phlorotannin chemotype dieckol (**8**) that significantly blocks the cleavage of a SARS-CoV 3CL^{pro}.

2.4. Real-time analysis of dieckol (**8**) interaction with SARS-CoV 3CL^{pro} by surface plasmon resonance (SPR)

Surface plasmon resonance (SPR) is a useful technique for monitor molecular reactions in real-time and has been used to determine binding specificity as well as the rates of association and dissociation between ligands and protein. In this study, the SARS-CoV 3CL^{pro} was immobilized on the sensor chip, and the most potent 3CL^{pro} inhibitor, dieckol (**8**), isolated from *E. cava* was passed over the sensor's surface. To analyze whether dieckol's (**8**) interaction is due to a specific binding event, the SPR sensorgram of the compound was recorded at several different concentrations. The binding responses in resonance units (RUs) were continuously recorded and presented graphically as a function of time. The associ-

ation was described by a simple equilibrium of the A + B ↔ AB type (A, analyte; B, ligand; and AB, complex). The SPR sensorgram was used to determine the kinetic binding parameters, the association rate constant k_{on} [μM⁻¹ s⁻¹] and the dissociation rate constant k_{off} [s⁻¹]. For SARS-CoV 3CL^{pro}, dieckol (**8**) increased the SPR sensorgram in a significant and dose-dependent manner (Fig. 4A). The dissociation constant K_D (k_{off}/k_{on}) was calculated by globally fitting the kinetic data at various dieckol (**8**) concentrations (12.5, 25, and 50 μM) to the Langmuir binding model ($K_D = 10.3$ μM). The K_D for the dieckol (**8**) interaction was thus simulated as a classical type of interaction (several analyte concentrations flowed serially across an immobilized ligand with a surface regeneration step between each infection)³⁴ with $k_{on} = 73.5$ μM⁻¹ s⁻¹ and $k_{off} = 0.000843$ s⁻¹, which quantitatively revealed a higher association rate than that of hesperetin ($K_D = 24.5$ μM) (see Supplementary data Fig. 7S).

2.5. In silico molecular docking simulation of dieckol (**8**)

The promising results outlined above encouraged us to further investigate the principal interactions between the phlorotannin and SARS-CoV 3CL^{pro}. To gain further insight into the inhibition mechanism, a docking experiment was performed. The most potent inhibitor of SARS-CoV 3CL^{pro}, dieckol (**8**), was analyzed by molecular docking analysis for its interactions with protein residues in the original ligand-binding site. The 3-dimensional structure of SARS-CoV 3CL^{pro} complex to an inhibitor (coded 2ZU5)³² obtained from the Protein Data Bank (PDB; <http://www.rcsb.org/pdb/>) was used for the modeling analysis. The conformation analysis was conducted using AutoDock 3.0.5 because of its powerful conformational search capabilities.

Phlorotannins (**1–9**), which have been identified as competitive inhibitors of the *trans/cis*-cleavage assays of SARS-CoV 3CL^{pro}, were fit into the substrate-binding pocket (S1 pocket) of the enzyme in the docking simulation. The results of the simulation showed that the tested compounds (**1–9**) had docking energies ranging from -5.83 to -11.76 kcal/mol (see Supplementary data Table 2S). Most poignantly, dieckol (**8**), which possess two eckol groups linked by a diphenyl ether, showed the lowest binding energy of -11.51 kcal/mol. Previously, we found that the eckol structure is essential and crucial for good inhibition of SARS-CoV 3CL^{pro}. As shown in Figure 4B, the C2'' hydroxyl group of dieckol (**8**) forms a hydrogen bond with Thr190 (4.66 Å), and the C5' hydroxyl group forms a hydrogen bond with His163 (2.87 Å). Additionally, the C3' hydroxyl group forms a hydrogen bond with Ser144 (2.78 Å), and the C2 hydroxyl group of dieckol (**8**) formed two H-bonds with His41 (2.79 Å) and Cys145 (3.41 Å), the catalytic residues of SARS-CoV 3CL^{pro}. Simulating the docking interactions between dieckol (**8**) and the amino acid residues in the active site of 3CL^{pro} revealed that dieckol (**8**) bound to the S1 site of SARS-CoV 3CL^{pro} through H-bonds. Additionally, we confirmed that dieckol (**8**) formed especially strong hydrogen bonds to the catalytic dyad (Cys145 and His41) of SARS-CoV 3CL^{pro}. These docking experiments support the inferences drawn from the enzymatic assay that revealed the important inhibitory action of dieckol (**8**) on SARS-CoV 3CL^{pro}.

3. Conclusions

In this study, we report for the first time that phlorotannins from *E. cava* competitively inhibited SARS-CoV 3CL^{pro} in the cell-free/based systems. The inhibition activities of phlorotannins against 3CL^{pro} were assessed with a cell-free/based analysis confirmed by FRET and luciferase. From these results, we evaluated the binding affinity of the phlorotannins isolated from *E. cava* for 3CL^{pro} by SPR analysis and a molecular binding study. All of the phlorotannins (**1–9**), except phloroglucinol (**1**), showed a dose-

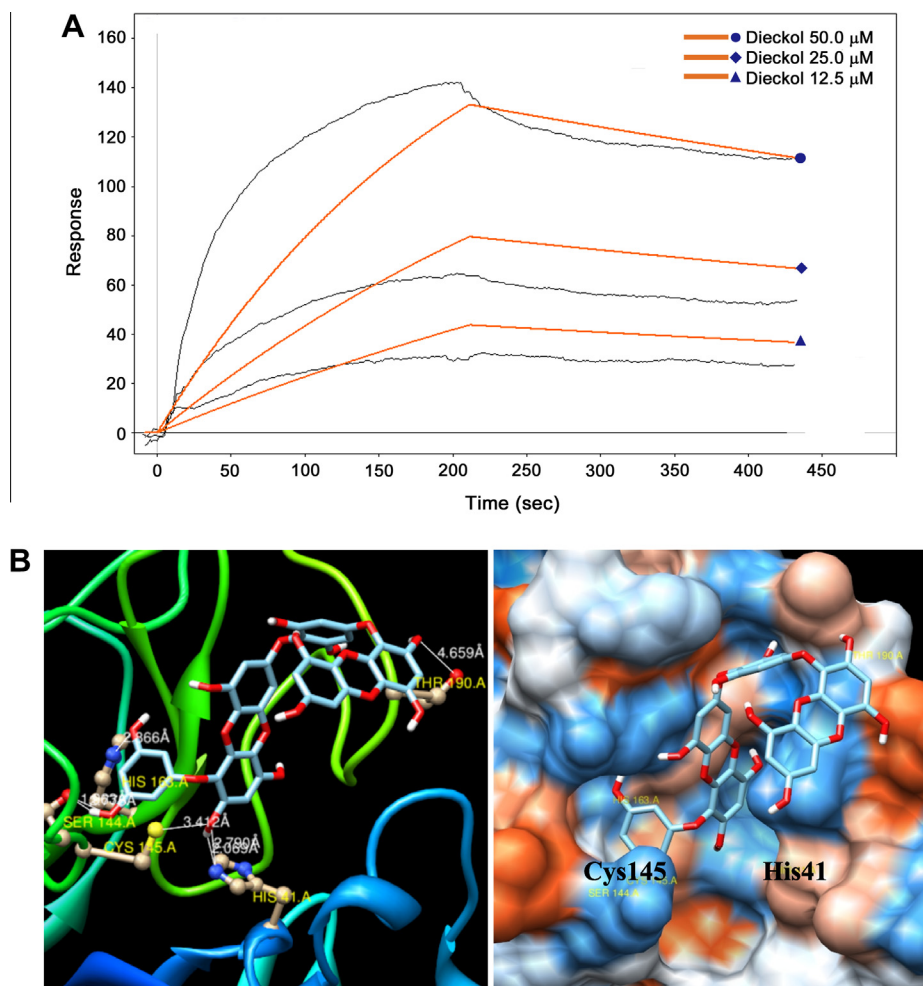


Figure 4. (A) Sensorgrams for the interaction of dieckol (**8**) with SARS-CoV 3CL^{Pro}. (B) The binding pose of dieckol (**8**) in SARS-CoV 3CL^{Pro}. Ribbon plots of dieckol (**8**) complexed to 3CL^{Pro} with hydrogen bonding.

dependent inhibitory effect on 3CL^{Pro} hydrolysis with IC₅₀ values ranging from 2.7 to 164.7 μM against cell-free 3CL^{Pro} *trans*-cleavage. All 3CL^{Pro} inhibitors (**2–9**) manifested competitive inhibition. In particular, dieckol (**8**), which possesses two Eckol groups linked by a diphenyl ether, showed the most potent SARS-CoV 3CL^{Pro} inhibitory activity (IC₅₀ = 2.7 μM). Additionally, dieckol (**8**) had the most potent inhibitory activity on the cell-based 3CL^{Pro} *cis*-cleavage assay, and its potency was greater than the other phlorotannin derivatives and the natural reference inhibitors. In addition, our detailed protein-inhibitor binding affinity analyses by SPR and molecular docking simulations of dieckol (**8**) unveiled that it has a high association rate and forms strong hydrogen bonds to the catalytic dyad (Cys145 and His41) of SARS-CoV 3CL^{Pro} with the lowest binding energy.

4. Materials and methods

4.1. General apparatus and chemical

¹H and ¹³C NMR data were obtained on a JNM-ECA 400 (Jeol, Japan) spectrometer in DMSO-*d*₆ and MeOH-*d*₃, and using tetramethylsilane (TMS) as an internal standard. ESI mass spectra were collected in negative ion mode. HPLC spectra were collected with an Agilent 1200 series equipped with a binary pump and VWD and analyzed with the Chemstation software program. The analytical column was an Agilent ZARBOX Bonus-RP (5 m, 150 × 4.6 mm

i.d.). All reagent grade chemicals were purchased from Sigma Chemical Co. (St. Louis, MO, USA). Chromatographic separations were carried out using Thin-Layer Chromatography (TLC) (E. Merck Co., Darmstadt, Germany) on commercially available glass plates pre-coated with silica gel and visualized under UV light at 254 and 366 nm. Column chromatography was carried out using 230–400 mesh silica gel (kieselgel 60, Merck, Germany). Sephadex LH-20 (Amersham Biosciences) and RP-18 (ODS-A, 12 nm, S-150 mM, YMC) were used for column chromatography.

4.2. Extraction and isolation

Dried powder of brown Alga *Ecklonia cava* (3 kg) was extracted with ethanol (3 × 15 L) for a week at room temperature. The concentrated extract (230 g) was suspended in H₂O (2 L), and the aqueous layer was partitioned sequentially with *n*-hexane (10 L), ethyl acetate (20 L), and water. The obtained ethyl acetate layer (85 g) was chromatographed over silica gel using a chloroform:methanol (100:0–1:3, v/v) gradient to produce 15 fractions (fr. 1–fr. 15). Fraction 4 (fr. 4) was repeatedly subjected to silica gel column chromatography using a mixture chloroform:methanol (100:0–1:3, v/v) to give 3 fractions (fr. 41–fr. 43). Dioxinohydroeckol (**4**) was purified from a sub-fraction (fr. 42) by MPLC using a gradient solvent system containing chloroform:methanol (100:0–7:3, v/v). Triphloretol-A (**2**) and dieckol (**8**) were obtained by purifying fraction 7 (fr. 7) using C-18 column chromatography

with a mixture of water:methanol (100:0–1:4, v/v). Fraction 5 (fr. 5) was purified on a silica gel column using a gradient solvent system containing chloroform:methanol (100:0–1:5, v/v) to yield 5 fractions (fr. 51–fr. 55) based on TLC analysis. Phlorofucofuroeckol A (**9**) was purified by MPLC using a chloroform:methanol solvent mixture (100:0–7:3, v/v) and was obtained from a sub-fraction (fr. 53). Fraction 55 (fr. 55) was subjected to C-18 column chromatography using water:methanol (100:0–1:4, v/v) to give 7-phloro- roeckol (**6**), fucodiphloroethol G (**7**) and eckol (**3**) based on TLC analysis. Fraction 51 (fr. 51) was re-purified through a C-18 column with methanol, and two compounds were obtained, phloroglucinol (**1**) and 2-phloro- roeckol (**5**).

4.3. Characteristic data of the isolated compounds

4.3.1. Phloroglucinol (**1**)

White powder; mp 218–219 °C; ESI-MS $m/z = 125$ [M–H][−], [calcd C₆H₆O₃, 126]; ¹H NMR (400 MHz, methanol-*d*₄) δ 5.80 (s, 3H, H-2, H-4, H-6); ¹³C NMR (75 MHz, methanol-*d*₄) δ 158.7 (C-1, C-3, C-5), 94.0 (C-2, C-4, C-6).

4.3.2. Triphlorethol A (**2**)

White powder; ESI-MS $m/z = 373$ [M–H][−], [calcd C₁₈H₁₄O₉, 374]; ¹H NMR (400 MHz, methanol-*d*₄) δ 6.06 (d, *J* = 2.93 Hz, 1H, H-5), 6.01 (d, *J* = 1.95 Hz, 2H, H-6, H-2''), 5.94 (t, *J* = 2.44 Hz, 1H, H-4''), 5.90 (s, 2H, H-5', H-3'), 5.76 (d, *J* = 2.44 Hz, 1H, H-3); ¹³C NMR (100 MHz, methanol-*d*₄) δ 162.5 (C-1''), 160.4 (C-3'', C-5''), 156.5 (C-4'), 156.3 (C-4), 153.8 (C-6), 152.7 (C-2), 152.2 (C-6', C-2'), 125.8 (C-1), 124.8 (C-1'), 98.2 (C-3), 97.6 (C-4''), 96.3 (C-5', C-3'), 95.5 (C-2'', C-6''), 95.0 (C-5).

4.3.3. Eckol (**3**)

Light brown powder; mp 235 °C; ESI-MS $m/z = 371$ [M–H][−], [calcd C₁₈H₁₂O₉, 372]; ¹H NMR (400 MHz, methanol-*d*₄) δ 6.15 (s, 1H, H-3), 5.96 (s, 2H, H-3, H-6), 6.03 (s, 3H, H-2', H-4', H-6'); ¹³C NMR (100 MHz, methanol-*d*₄) δ 161.9 (C-1'), 160.3 (C-3', H-5'), 154.6 (C-7), 147.3 (C-2), 147.2 (C-9), 144.3 (C-5a), 143.4 (C-4), 138.6 (C-10a), 125.7 (C-1), 124.9 (C-4a), 124.6 (C-9a), 99.9 (C-8), 99.5 (C-3), 97.8 (C-4'), 95.9 (C-6), 95.5 (C-4', C-6').

4.3.4. Dioxinodehydroeckol (**4**)

White powder; ESI-MS $m/z = 371$ [M+H]⁺, [calcd C₁₈H₁₀O₉, 370]; ¹H NMR (400 MHz, methanol-*d*₄) δ 6.15 (s, 1H, H-7), 6.02 (d, *J* = 2.93 Hz, 1H, H-2), 6.01 (d, *J* = 2.44 Hz, 1H, H-10), 5.99 (d, *J* = 2.93 Hz, 1H, H-4), 5.96 (d, *J* = 2.93 Hz, 1H, H-12); ¹³C NMR (100 MHz, methanol-*d*₄) δ 147.3 (C-1), 147.2 (C-9), 144.0 (C-4a), 143.7 (C-12a), 141.5 (C-6), 139.4 (C-7a), 133.3 (C-13b), 128.0 (C-5a), 125.1 (C-8a), 125.0 (C-13a), 124.7 (C-14a), 100.2 (C-2), 100.0 (C-10), 99.1 (C-7), 96.0 (C-4), 96.0 (C-5).

4.3.5. 2-Phloro- roeckol (**5**)

Light brown powder; mp 201–205 °C; ESI-MS $m/z = 495$ [M–H][−], [calcd C₂₄H₁₆O₁₂, 495]; ¹H NMR (400 MHz, DMSO-*d*₆) δ 9.51 (s, 1H, OH-9), 9.40 (s, 1H, OH-4), 9.17 (s, 1H, OH-7), 9.12 (s, 1H, OH-3', 5''), 9.07 (s, 1H, OH-2'', 6''), 8.96 (s, 1H, OH-4''), 5.97 (d, *J* = 2.93 Hz, 1H, H-8), 5.86 (d, *J* = 1.95 Hz, 2H, H-2', 6'), 5.84 (s, 2H, H-3'', 5''), 5.82 (t, *J* = 1.95 Hz, 1H, H-4'), 5.81 (s, 1H, H-3), 5.79 (d, *J* = 2.93 Hz, 1H, H-5); ¹³C NMR (100 MHz, DMSO-*d*₆) δ 159.9 (C-1'), 158.3 (C-3', C-5'), 154.3 (C-4'), 152.7 (C-7), 150.7 (C-2'', H-6''), 147.3 (C-2), 145.7 (C-9), 142.1 (C-5a), 141.2 (C-4), 136.7 (C-10a), 123.8 (C-4a), 122.2 (C-1), 121.4 (C-9a), 98.2 (C-8), 95.9 (C-4'), 95.5 (C-3), 94.4 (C-3'', 5''), 93.7 (C-2', C-6'), 93.4 (C-6).

4.3.6. 7-Phloro- roeckol (**6**)

Light brown powder; ESI-MS $m/z = 495$ [M–H][−], [calcd C₂₄H₁₆O₁₂, 496]; ¹H NMR (400 MHz, DMSO-*d*₆) δ 9.60 (s, 1H, OH-

9), 9.40 (s, 1H, OH-4), 9.20 (s, 1H, OH-2), 9.12 (s, 1H, OH-3', 5'), 9.11 (s, 1H, OH-2'', 6''), 8.99 (s, 1H, OH-4'), 6.14 (s, 1H, H-3), 6.00 (d, *J* = 2.93 Hz, 1H, H-8), 5.85 (s, 2H, H-3'', 5''), 5.80 (t, *J* = 1.95 Hz, 1H, H-4'), 5.78 (d, *J* = 2.93 Hz, 1H, H-6), 5.85 (d, *J* = 2.44 Hz, 2H, H-2', 6'); ¹³C NMR (100 MHz, DMSO-*d*₆) δ 160.2 (C-1'), 158.7 (C-3', C-5'), 154.7 (C-4'), 154.5 (C-7), 151.1 (C-2'', H-6''), 146.0 (C-9), 145.8 (C-2), 142.3 (C-5a), 141.8 (C-4), 137.0 (C-10a), 123.9 (C-9a), 123.1 (C-4a), 122.1 (C-1''), 122.1 (C-1), 98.2 (C-3), 98.1 (C-8), 96.2 (C-4'), 94.8 (C-3''), 93.6 (C-2').

4.3.7. Fucodiphloroethol G (**7**)

White powder; ESI-MS $m/z = 499$ [M+H]⁺, [calcd C₂₄H₁₆O₁₂, 498]; ¹H NMR (400 MHz, methanol-*d*₄) δ 6.13 (d, *J* = 2.44 Hz, 1H, H-4''), 6.07 (s, 2H, H-3''', H-5'''), 6.03 (s, 1H, H-6''), 6.03 (d, *J* = 0.98 Hz, 1H, H-5), 5.92 (s, 2H, H-3', H-5'), 5.70 (d, *J* = 2.44 Hz, 1H, H-3); ¹³C NMR (100 MHz, methanol-*d*₄) δ 159.6 (C-5''), 159.5 (C-1''), 159.3 (C-3''), 159.2 (C-4'''), 158.1 (C-4'), 157.6 (C-2), 156.5 (C-2''', C-6'''), 153.9 (C-4), 152.3 (C-2', C-6'), 152.1 (C-6), 124.9 (C-1), 124.4 (C-1'), 102.1 (C-2''), 101.9 (C-1'''), 98.1 (C-3), 97.6 (C-4''), 96.8 (C-5'''), 96.4 (C-3''', C-5', C-3'), 94.6 (C-5), 94.3 (C-6'').

4.3.8. Dieckol (**8**)

Light brown powder; mp 278 °C; ESI-MS $m/z = 741$ [M–H][−], [C₃₀H₁₈O₁₄, 742]; ¹H NMR (400 MHz, methanol-*d*₄) δ 6.16 (s, 1H, H-3''), 6.14 (s, 1H, H-3), 6.10 (s, 2H, H-2''', H-6'''), 6.07 (d, 1H, *J* = 2.93 Hz, H-6), 6.06 (d, 1H, *J* = 2.93 Hz, H-8), 5.99 (d, 1H, *J* = 2.93 Hz, H-6''), 5.96 (d, 1H, *J* = 2.93 Hz, H-8''), 6.10 (s, 3H, H-4', H-2' H-6'); ¹³C NMR (C-7'''), 152.5 (C-3''', C-5'''), 147.5 (C-2), 147.4 (C-9'), 147.3 (C-9''), 147.1 (C-2''), 144.4 (C-5a''), 144.3 (C-5a), 143.5 (C-4), 143.4 (C-4a''), 138.8 (C-10a), 138.6 (C-10a'), 126.6 (C-4'''), 126.3 (C-9a), 125.8 (C-4a), 125.7 (C-4a''), 125.0 (C-9a''), 124.8 (C-1''), 124.7 (C-1), 100 (C-8''), 99.9 (C-3''), 99.6 (C-3), 99.5 (C-8), 97.8 (C-4'), 96.3 (C-2''', C-6'''), 96.0 (C-6''), 95.9 (C-6), 95.5 (C-2', C-6'').

4.3.9. Phlorofucofuroeckol A (**9**)

Colorless amorphous solid; mp 278 °C; ESI-MS $m/z = 601$ [M–H][−], [calcd C₃₀H₁₈O₁₄, 602]; ¹H NMR (400 MHz, methanol-*d*₄) δ 6.64 (s, 1H, H-13), 6.41 (s, 1H, H-9), 6.27 (s, 1H, H-3), 6.07 (d, 1H, *J* = 2.93 Hz, H-6), 5.99 (d, 2H, *J* = 1.95 Hz, H-2', H-6'), 5.95 (t, 1H, *J* = 1.95 Hz, H-4'), 5.93 (t, 1H, *J* = 1.95 Hz, H-4''), 5.90 (d, 2H, *J* = 1.95 Hz, H-2'', H-6''); ¹³C NMR (100 MHz, methanol-*d*₄) δ 162.0 (C-1', C-1''), 160.3 (C-3'', C-5'', C-3', C-5'), 153.3 (C-12a), 151.8 (C-10), 151.3 (C-11a), 146.1 (C-14), 144.1 (C-4), 138.5 (C-15a), 135.4 (C-5a), 128.3 (C-14a), 125.2 (C-4a), 124.8 (C-1), 122.5 (C-11), 105.5 (C-7), 105.4 (C-6), 100.1 (C-9), 99.5 (C-3), 97.9 (C-4''), 97.8 (C-4'), 96.3 (C-13), 95.5 (C-2', C-6', C-2'', C-6'').

4.4. Expression and purification of SARS-CoV 3CL^{Pro}

The gene encoding the 3CL protease (nucleotide residues 9970–10887, GenBank accession no. AY345987) of SARS-CoV was synthesized based on the sequence reported by Sun et al.²⁵ (GenScript, Piscataway, NJ, USA). Recombinant SARS-CoV 3CL^{Pro} was expressed *E. coli* BL21 (DE3) CodonPlus-RIL cells (Stratagene, La Jolla, CA, USA) by transforming the pET23d(+)-SARS-3CL^{Pro} to produce a C-terminal fusion with six histidine residues. The expression and purification of SARS-CoV 3CL^{Pro} were performed as previously described.^{26,27} Briefly, cells were grown in 1 L of LB broth containing 100 μg/ml of ampicilline at 37 °C until OD₆₀₀ reached 0.5 and were then induced with 0.5 mM isopropyl β-D-thiogalactopyranoside for 8 h at 16 °C. After centrifugation at 6000 ×g at 4 °C for 25 min, the pellet was washed, frozen, and suspended in buffer A (20 mM sodium phosphate, 300 mM NaCl, 10 mM imidazole, 0.1% Triton X-100, pH 7.5). The suspended cells were sonicated and centrifuged at 15,000 ×g at 4 °C for 30 min.

The resulting supernatant was applied to a nickel-affinity chromatography throughout the procedure. The protein in the final column fraction was dialyzed overnight against 20 mM Tris–HCl buffer (pH 7.5) with 1 mM dithiothreitol and stored at -80°C . The enzyme concentration was determined spectrophotometrically at 562 nm using the BioRad protein assay. The purity and molecular weight of SARS-CoV 3CL^{pro} was verified by SDS–PAGE. The purified protease ran approximately to the calculated size of 33 kDa on SDS–PAGE.

4.5. SARS-CoV 3CL^{pro} trans-cleavage assay

As described, the inhibitory effect of each compound on SARS-CoV 3CL^{pro} was measured using a FRET method.^{26,27} In this assay, the 14-mer fluorogenic peptide Dabcyl-KTSAVLQSGFRKME-Edans (Anygen Co., Republic of Korea) was used as a substrate, and the enzyme activity was determined by measuring the increase in fluorescence by continuously monitoring the reactions at 590/40 nm with excitation at 360 nm using a fluorescence plate reader (Flx800, BioTeck Instrument Inc., USA). The IC₅₀ values of the isolated compounds were measured in a reaction mixture containing 10 μg/ml of the 3CL^{pro} (final concentration, 2.5 μg), the test compounds (from 0 to 200 μM), and 10 μM of the fluorogenic 14-mer peptide substrate in 20 mM Bis–Tris buffer (pH 7.5). To determine the enzyme activity, the experimental data was fit to a logistic curve with Eq. 1, a time-drive protocol was used and the initial velocity was recorded over a range of concentrations, and the data were analyzed using a nonlinear regression program [Sigma Plot (SPCC Inc., Chicago, IL)]:

$$\text{Inhibition activity (\%)} = 100 - [(S - S_0)/(C - C_0)] \times 100 \quad (1)$$

where C is the fluorescence of the control (enzyme, buffer, and substrate) after 60 min of incubation, C₀ is the fluorescence of the control at 0 min, S is the fluorescence of the tested samples (enzyme, sample solution, and substrate) after incubation, and S₀ is the fluorescence of the tested samples at 0 min.

To study the kinetics of SARS-CoV 3CL^{pro} inhibition by isolated compounds 1–9, various concentrations of compounds 1–9 were added to 3CL^{pro} in assay buffer containing the predetermined substrate. The K_i values were calculated by nonlinear regression analysis by fitting different models of enzyme inhibition to the kinetic data using SigmaPlot Enzyme Kinetics Module 1.3 (SPSS Inc., Chicago, IL). The inhibition mechanism of the compounds was determined by comparing the statistical results, including the Akaike's information criterion values, of different inhibition models and selecting the one with the best fit.²⁸

4.6. SARS-CoV 3CL^{pro} cis-cleavage assay

For the cell-based cis-cleavage assay, the in-frame construction of 3CL^{pro}, the substrate, and luciferase formed the plasmid pcDNA3.1–3CL^{pro}–S–Luc.^{22,29} The constructed plasmid DNA was transfected into Vero cells with lipofectamin according to the manufacturer's instructions (Invitrogen, USA). The transfected cells were incubated in Dulbeccos modified Eagle's medium (DMEM) containing 10% bovine serum (FBS) for 4 h at 37 °C under a 5% CO₂ atmosphere. Then, the media was removed and replaced by DMEM containing the tested compounds at different concentrations. After 5 h of incubation, the activity of luciferase in the cell lysate was measured using the dual Luciferase Reporter Assay System (Promega, USA) and a Luminometer Centro XS³ LB 960 (Berthold Technology, Inc.). Because the greater than 33 kDa protein fused to the N-terminus of luciferase remarkably decreased luciferase activity,³⁰ the detection of luciferase activity was considered a measure of the cis-cleavage by the SARS-CoV 3CL^{pro}.²²

4.7. Real-time analysis of ligand interaction with SARS-CoV 3CL^{pro} by surface plasmon resonance (SPR)

SPR measurements were performed on a Reichert SPR SR7500 instrument kindly provided on loan from Woojung BSC Inc. The enzyme was dialyzed in PBS buffer prior to immobilization. The surface was activated with a 7 min injection of EDC/sulfo-NHS mixture at 200/50 mM concentration. The protein was diluted to 100 μg/mL with 20 mM acetate buffer (pH 5.0) and injected for 10 min. The active sites were quenched with 1 M ethanolamine buffer at pH 8.0 and washed with phosphate-buffered saline at pH 7.2 (PBS). The binding surface was stabilized with 3–5 blank injections of PBS. PBS was used as a running and sample dilution buffer for all of the experiments. The tested inhibitors were first prepared as 20 mM stock solutions in dimethyl sulfoxide (DMSO) and further diluted into PBS immediately prior to the experiments. Analyte binding was analyzed using automated runs of the twofold dilution series and two 'zero concentration' injections. Regeneration steps were performed using 10 mM NaOH. The data was analyzed with the Scrubber2 software. Referenced and blanked binding dissociation curves were fit globally to a two-state binding kinetics model.

4.8. Molecular docking simulation study

Docking experiments were conducted using Autodock 3.0.5 with a Lamarckian Genetic Algorithm (LGA).³¹ A 3-dimensional coordinate in the X-ray crystal structure of SARS-CoV 3CL^{pro} (PDB accession code 2ZU5)³² obtained from the Protein Data Bank (PDB; <http://www.pdb.org>) was used for the docking studies. After removing the water molecules, the polar hydrogen (H) atoms were added to the macromolecule, the histidine residues were made neutral, and the Kollman charges were assigned for all atoms.³³ The 3-dimensional atomic coordinates of the compounds were generated by the Corina program (Molecular Networks GmbH, Erlangen, Germany). AutoDock version 3.0.5 was used for the computational molecular docking simulation of the flexible small molecules to the rigid proteins. The docking results were ranked according to the docking energy scores. The Chimera software 1.4.1 program (University of California, San Francisco) was used to identify the potential H-bonds between the residues in the active site pocket of SARS-CoV 3CL^{pro}.

Acknowledgments

This research was supported by National Research Foundation Grant founded by Korea Government (MEST) (No. 2012-0001110) and KRIBB Research Initiative Program, Republic of Korea.

Supplementary data

Supplementary data associated with this article can be found, in the online version, at <http://dx.doi.org/10.1016/j.bmc.2013.04.026>.

References and notes

- Jung, W.-K.; Heo, S.-J.; Jeon, Y.-J.; Lee, C.-M.; Park, Y.-M.; Byun, H.-G.; Choi, Y. H.; Park, S.-G.; Choi, I.-W. *J. Agric. Food Chem.* **2009**, *57*, 4439.
- Kim, K. N.; Heo, S. J.; Yoon, W. J.; Kang, S. M.; Ahn, G.; Yi, T. H.; Jeon, Y. J. *Eur. J. Pharmacol.* **2010**, *649*, 369.
- Lee, S.-H.; Heo, S.-J.; Hwang, J.-Y.; Han, J.-S.; Jeon, Y.-J. *J. Sci. Food Agric.* **2010**, *90*, 349.
- Choi, J.-G.; Kang, O.-H.; Brice, O.-O.; Lee, Y.-S.; Chae, H.-S. C.; Oh, Y.-C.; Sohn, D.-H.; Park, H.; Choi, H.-G.; Kim, S.-G.; Shin, D.-W.; Kwon, D.-Y. *Foodborne Pathog. Dis.* **2010**, *7*, 436.
- Zeng, C.; Teseng, C.; Zhang, J.; Chang, C. *Hydrobiologia* **1984**, *116*, 152.

6. Ahn, G.-N.; Kim, K.-N.; Cha, S.-H.; Song, C.-B.; Lee, J.; Heo, M.-S.; Yeo, I.-K.; Lee, N.-H.; Jee, Y.-H.; Kim, J.-S.; Heu, M.-S.; Jeon, Y.-J. *Eur. Food Res. Technol.* **2007**, *226*, 71.
7. Kim, M.-M.; Ta, Q. V.; Mendis, E.; Rajapakse, N.; Jung, W.-K.; Byun, H.-G.; Jeon, Y.-J.; Kim, S.-K. *Life Sci.* **2006**, *79*, 1436.
8. Crockett, S. L.; Wenzig, E. M.; Kunert, O.; Bauer, R. *Phytochem. Lett.* **2008**, *1*, 37.
9. Kang, K. A.; Lee, K. H.; Park, J. W.; Lee, N. H.; Na, H. K.; Surh, Y. J.; You, H. J.; Chung, M. H.; Hyun, J. W. *FEBS Lett.* **2000**, *2007*, 581.
10. Yoon, N. Y.; Eom, T. K.; Kim, M. M.; Kim, S. K. *J. Agric. Food Chem.* **2009**, *57*, 4124.
11. Artan, M.; Li, Y.; Karadeniz, F.; Lee, S.-H.; Kim, M.-M.; Kim, S.-K. *Bioorg. Med. Chem.* **2008**, *16*, 7921.
12. Ryu, Y. B.; Jeong, H. J.; Yoon, S. Y.; Park, J.-Y.; Kim, Y. M.; Park, S.-J.; Rho, M.-C.; Kim, S.-J.; Lee, W. S. *J. Agric. Food Chem.* **2011**, *59*, 6467.
13. Ksiazek, T. G.; Erdman, D.; Goldsmith, C. S.; Zaki, S. R.; Peret, T.; Emery, S.; Tong, S.; Urbani, C.; Comer, J. A.; Lim, W.; Rollin, P. E.; Dowell, S. F.; Ling, A.-E.; Humphrey, C. D.; Shieh, W.-J.; Guarner, J.; Paddock, C. D.; Rota, P.; Fields, B.; DeRisi, J.; Yang, J.-Y.; Cox, N.; Hughes, J. M.; LeDuc, J. W.; Bellini, W. J.; Anderson, L. J. *N. Eng. J. Med.* **2003**, *348*, 1953.
14. Stadler, K.; Masignani, V.; Eickmann, M.; Becker, S.; Abrignani, S.; Klenk, H. D.; Rappuoli, R. *Nat. Rev. Microbiol.* **2003**, *1*, 209.
15. Ziebuhr, J. *Curr. Opin. Microbiol.* **2004**, *7*, 412.
16. Yang, H.; Yang, M.; Ding, Y.; Liu, Y.; Lou, Z.; Zhou, Z.; Sun, L.; Mo, L.; Ye, S.; Pang, H.; Gao, G. F.; Anand, K.; Bartlam, M.; Hilgenfeld, R.; Rao, Z. *Proc. Natl. Acad. Sci. U.S.A.* **2003**, *100*, 13190.
17. Cinatl, J., Jr.; Michaelis, M.; Hoever, G.; Preiser, W.; Doerr, H. W. *Antiviral Res.* **2005**, *66*, 81.
18. Wu, C. Y.; Jan, J. T.; Ma, S. H.; Kuo, C. J.; Juan, H. F.; Cheng, Y. S.; Hsu, H. H.; Huang, H. C.; Wu, D.; Brik, A.; Liang, F. S.; Liu, R. S.; Fang, J. M.; Chen, S. T.; Liang, P. H.; Wong, C. H. *Proc. Natl. Acad. Sci. U.S.A.* **2004**, *101*, 10012.
19. Kao, R. Y.; Tsui, W. H. W.; Lee, T. S. W.; Tanner, J. A.; Watt, R. M.; Huang, J.-D.; Hu, L.; Chen, G.; Chen, Z.; Zhang, L.; He, T.; Chan, K.-H.; Tse, H.; To, A. P. C.; Ng, L. W. Y.; Wong, B. C. W.; Tsoi, H.-W.; Yang, D.; Ho, D. D.; Yuen, K.-Y. *Chem. Biol.* **2004**, *11*, 1293.
20. Shie, J. J.; Fang, J. M.; Kuo, C. J.; Kuo, T. H.; Liang, P. H.; Huang, H. J.; Yang, W. B.; Lin, C. H.; Chen, J. L.; Wu, Y. T.; Wong, C. H. *J. Med. Chem.* **2005**, *48*, 4469.
21. Wen, C.; Kuo, Y.; Jan, J.; Liang, P.; Wang, S.; Liu, H.; Lee, C.; Chang, S.; Kuo, C.; Lee, S.; Hou, C.; Hsiao, P.; Chien, S.; Shyur, L.; Yang, N. *J. Med. Chem.* **2007**, *50*, 4087.
22. Lin, C. W.; Tsai, F. J.; Tsai, C. H.; Lai, C. C.; Wan, L.; Ho, T. Y.; Hsieh, C. C.; Chao, P. D. *Antiviral Res.* **2005**, *68*, 36.
23. Ryu, Y. B.; Park, S. J.; Kim, Y. M.; Lee, J. Y.; Seo, W. D.; Chang, J. S.; Park, K. H.; Rho, M. C.; Lee, W. S. *Bioorg. Med. Chem. Lett.* **2010**, *20*, 20.
24. Ryu, Y. B.; Jeong, H. J.; Kim, J. H.; Kim, Y. M.; Park, J.-Y.; Kim, D.; Nguyen, T. T.; Park, S.-J.; Chang, J. S.; Park, K. H.; Rho, M.-C.; Lee, W. S. *Bioorg. Med. Chem.* **2010**, *18*, 7940.
25. Sun, H.; Luo, H.; Yu, C.; Sun, T.; Chen, J.; Peng, S.; Qin, J.; Shen, J.; Yang, Y.; Xie, Y.; Chen, K.; Wang, Y.; Shen, X.; Jiang, H. *Protein Expression Purif.* **2003**, *32*, 302.
26. Park, J.-Y.; Jeong, H. J.; Kim, J. H.; Kim, Y. M.; Park, S.-J.; Kim, D.; Park, K. H.; Lee, W. S.; Ryu, Y. B. *Biol. Pharm. Bull.* **2012**, *35*, 2036.
27. Park, J.-Y.; Kim, J. H.; Kim, Y. M.; Jeong, H. J.; Kim, D. W.; Park, K. H.; Kwon, H.-J.; Park, S.-J.; Lee, W. S.; Ryu, Y. B. *Bioorg. Med. Chem.* **2012**, *20*, 5928.
28. Li, X.-Q.; Andersson, T. B.; Ahlström, M.; Weidolf, L. *Drug Metab. Dispos.* **2004**, *32*, 821.
29. Lin, C. W.; Tsai, C. H.; Tsai, F. J.; Chen, P. J.; Lai, C. C.; Wan, L.; Chiu, H. H.; Lin, K. H. *FEBS Lett.* **2004**, *574*, 131.
30. Joubert, P.; Pautigny, C.; Madelaine, M. F.; Rasschaert, D. *J. Gen. Virol.* **2000**, *81*, 481.
31. Morris, G. M.; Goodsell, D. S.; Halliday, R. S.; Huey, R.; Hart, W. E.; Belew, R. K.; Olson, A. J. *J. Comput. Chem.* **1998**, *19*, 1639.
32. Lee, C. C.; Kuo, C. J.; Ko, T. P.; Hsu, M. F.; Tsui, Y. C.; Chang, S. C.; Yang, S.; Chen, S. J.; Chen, H. C.; Hsu, M. C.; Shih, S. R.; Liang, P. H.; Wang, A. H. *J. Biol. Chem.* **2009**, *284*, 7646.
33. Sanner, M. F.; Olson, A. J.; Spehner, J. C. *Biopolymers* **1996**, *38*, 305.
34. Tassa, C.; Duffner, J. L.; Lewis, T. A.; Weissleder, R.; Schreiber, S. L.; Koehler, A. N.; Shaw, S. Y. *Bioconjugate Chem.* **2010**, *21*, 14.